An Optimized Control Scheme to Reduce the Backflow Power and Peak Current in Dual Active Bridge Converters

Liu, Bochen; Davari, Pooya; Blaabjerg, Frede

Published in:
Proceedings of 2019 IEEE Annual Applied Power Electronics Conference and Exposition (APEC 2019)

DOI (link to publication from Publisher):
10.1109/APEC.2019.8722273

Publication date:
2019

Document Version
Accepted author manuscript, peer reviewed version

An Optimized Control Scheme to Reduce the Backflow Power and Peak Current in Dual Active Bridge Converters

Bochen Liu, Pooya Davari, Frede Blaabjerg
Department of Energy Technology
Aalborg University
Aalborg, Denmark
bli@et.aau.dk, pda@et.aau.dk, fbl@et.aau.dk

***Abstract*—An optimized switching control scheme to reduce the backflow power and the peak current of the dual active bridge converter is presented in this paper. Based on a triple-phase-shift modulation, the control scheme consists of operating the switching devices with three optimized control variables on the basis of achieving a decreased backflow power and peak current. This can enhance the converter efficiency and reduce the current stress on the switching devices. The optimal values of these three manipulated variables are obtained through analysis of different operation modes. Besides, the power transfer ranges and soft-switching constraints are also explained in detail. Experimental results are presented to validate the feasibility of the proposed method.**

Keywords—dual active bridge, backflow power, current stress, triple-phase-shift

I. INTRODUCTION

The bidirectional isolated Dual Active Bridge (DAB) converter is now widely used in many applications such as electric vehicles and distributed power systems to adapt different voltage levels and control the power flow among multiple energy sources [1]-[4]. The advantages of high efficiency, galvanic isolation and bidirectional power flow make it also as a potential candidate for the future charging systems and vehicle-to-grid (V2G) power transfer.

With the everlasting need of higher converter efficiency and power density, over the years many modulation and control strategies have been introduced for DAB converters. For instance, extended phase-shift (EPS) [5], dual phase-shift (DPS) [6]-[8] and triple phase-shift (TPS) [9] modulation methods are proposed to replace the conventional single phase-shift (SPS) modulation, which is simple but having a limited soft-switching range. Therein, the TPS modulation has the highest degree of freedom, and the other modulation methods can be seen as particular cases of the TPS. At the control level, several optimal control strategies can be found in [10]-[12] where reducing the rms value of the leakage inductance current [10], [11] and suppressing the backflow power [12] are commonly used optimization objectives. In most papers, usually one optimization objective is selected to enhance the converter performance. For example, the current stress selected as the optimization target is minimized in [13] whereas the backflow power is considered in [14]. In fact, in terms of TPS modulation, multi-objective optimization is feasible since the TPS has three control variables, which is not addressed in the prior-art research studies.

Different from single-objective optimization, this paper proposes a TPS-based multi-objective optimization control scheme to simultaneously reduce the backflow power and the peak value of the leakage inductance current to improve the system efficiency and reduce the current stress on power semiconductors. By means of analytical calculations, the proposed control scheme can extract the optimal modulation parameters for the DAB converter in a wide voltage range. Firstly, the basic operation modes of the DAB converter are explained in Section II, and then the soft-switching constraints and power transfer range analysis are presented in Section III. Next, the proposed control method to simultaneously reduce the backflow power and the peak leakage inductance current is clarified in Section IV. In Section V, the laboratory prototype and experimental results are illustrated to validate the feasibility of the proposed control scheme. Finally, conclusions are summarized in Section VI.

II. DAB OPERATION MODES

The DAB converter topology is shown in Fig. 1, consisting of two full-bridges on the primary and secondary side of the high-frequency transformer. Usually an auxiliary inductor is put in series with the transformer to serve as part of the equivalent leakage inductance. The intermediate transformer has a turns ratio of n : 1 corresponding to the high-voltage (HV) input and low-voltage (LV) output.

In this paper, the DAB works in voltage boosting mode ($V_1/n < V_2$) and due to the converter symmetry, only positive power transmission is analyzed, namely from the primary high-voltage input to the secondary low-voltage output. In addition, the base value of the power P_b and voltage V_b defined in (1) are used to simplify the calculations. L is the equivalent leakage inductance of the transformer after referring to the primary side and f_{sw} is the switching frequency. The voltage ratio k is introduced as V_1/nV_2, which is within (0, 1).

$$P_b = \left(nV_2\right)^2 \Big/ 8Lf_{sw} \qquad I_b = nV_2 \Big/ 8Lf_{sw} \tag{1}$$

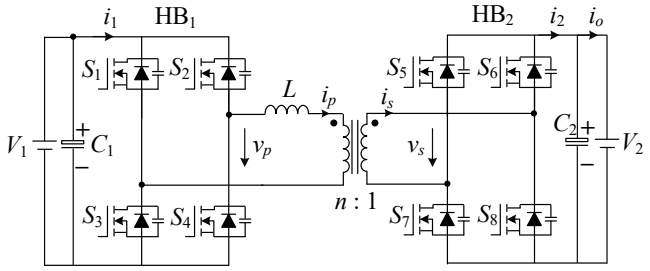

Fig. 1 Dual-active-bridge (DAB) converter topology

Taking the power transfer direction and voltage boosting into account, the DAB converter can work in four operation modes with TPS modulation [10]. However, as one mode would lead to an increased inductor rms current and does not result in a higher DAB power transfer capability [15], this paper will focus on three operation modes, namely Mode I, Mode II and Mode III as shown in Fig. 2. Therein, D_p, D_s are the duty cycle for the primary voltage v_p and secondary v_s, and D_φ denotes the phase-shift angle between v_p and v_s. Each power semiconductor is switched with a 50% duty cycle and the different shifted phases among these switching signals produce numerous values of D_p, D_s and D_φ.

Due to the phase-shift operation, only a portion of the power is consumed by the load while the other portion is sent back to the input capacitor C_1, which is called backflow power, as represented by the shaded area in Fig. 2. In order to calculate the average backflow power in half of the switching period, it is necessary to analyze the leakage inductance current first. As shown in Fig. 2(a), the slopes of the leakage inductance current i_L are ruled by the difference between the primary voltage v_p and the secondary voltage v_s, which is expressed in (2).

$$L\frac{di_L(t)}{dt} = v_p(t) - v_s(t) \tag{2}$$

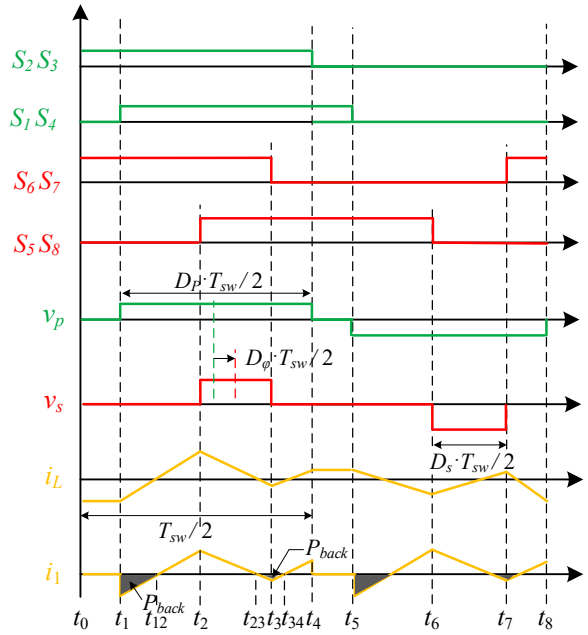

(a)

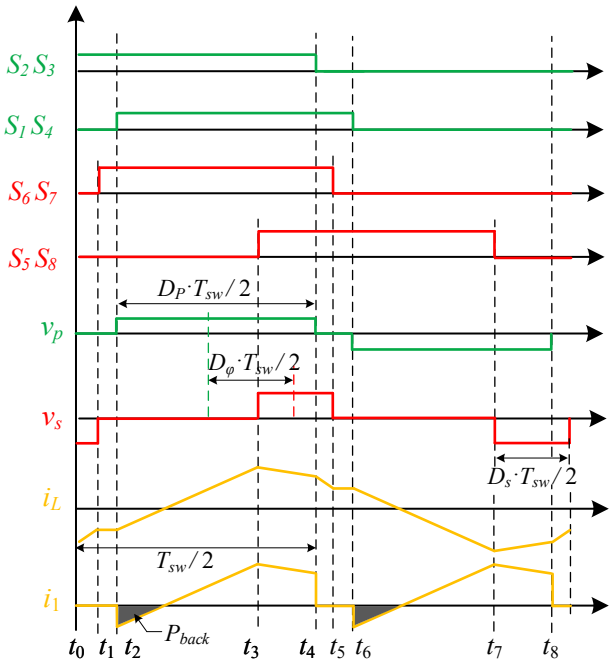

(b)

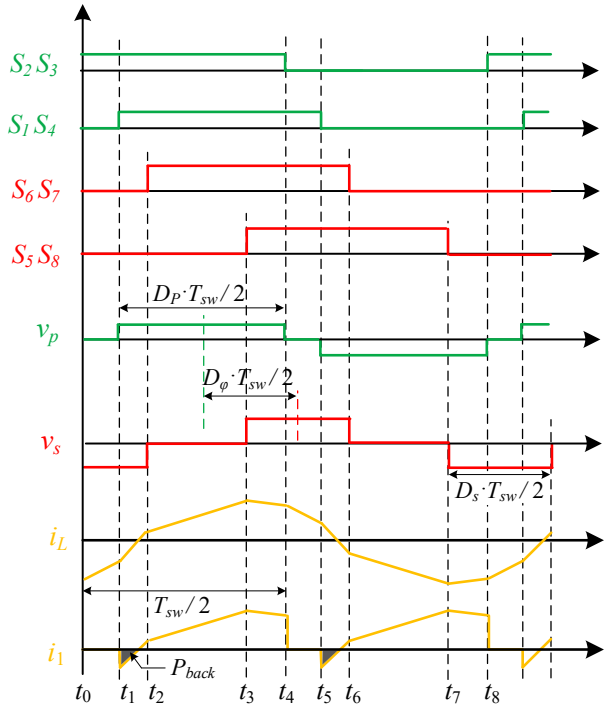

(c)

Fig. 2 Operation modes of DAB converters under TPS modulation: (a) Mode I (b) Mode II (c) Mode III

During the four switching intervals in half switching period, i.e. [t_0, t_1], [t_1, t_2], [t_2, t_3], [t_3, t_4], different equations can be derived according to (2), and the zero-crossing instants, i.e. t_{12}, t_{23}, t_{34} also can be obtained in conjunction with the volt-second balance of the leakage inductor. Thus, the average backflow power in half switching period can be calculated as

$$P_{back}=\frac{2V_1}{P_b\cdot T_{sw}}\cdot\left(\int_{t_1}^{t_{12}}\left|i_L(t)\right|dt+\int_{t_{23}}^{t_{34}}\left|i_L(t)\right|dt\right) \tag{3}$$

which is the normalized result considering the reference power P_b.

On the other hand, it can be seen that the peak leakage inductance current appears at the moment of t_2 in Fig. 2(a), and the normalized value is

$$I_{L,peak}=\frac{i_L(t_2)}{I_b} \tag{4}$$

The average backflow power and peak leakage inductance current in the other two modes can also be derived in a similar way based on the working waveforms in Fig. 2(b) and Fig. 2(c).

Besides, in order to appraise the power transfer ability of each operation mode in the following section, the average transmission power in half switching period is needed, which can be obtained by

$$P_o=\frac{2nV_2\cdot\left|\int_{t_r}^{t_f}i_L(t)dt\right|}{T_{sw}\cdot P_b} \tag{5}$$

In (5), t_r and t_f are the point of the rising edge and falling edge of the secondary voltage v_s in half switching period, i.e. [t_r t_f] is [t_2 t_3], [t_3 t_5] and [t_3 t_6] for Mode I, Mode II and Mode III, respectively.

Based on (2)-(5), the derived average transmission power P_o, the backflow power P_{back} and the peak leakage inductance current $I_{L,peak}$ for each operation mode are summarized in Table I with respect to the voltage ratio k and the three control variables D_p, D_s, D_φ.

III. Soft-Switching Constraints and Power Transfer Range

As shown in Fig. 2, the rising and falling edges of the primary voltage v_p and the secondary voltage v_s are interleaved along the time axis. For each operation mode, the relative position relationship of the voltage edges are totally determined by the three control variables D_p, D_s and D_φ. Therefore, the operating modes boundaries also can be depicted with these three variables. Seen from Fig. 2(a) to Fig. 2(c), the phase-shift angle between the primary and secondary voltage is an effective factor provoking the three different operation modes. Therefore, with the shift of D_φ, the DAB converter can work in corresponding mode, as expressed in the second column of Table II. It should be noted that there are some universal limits on the three control variables.

According to the definition in Section II, it can be easily drawn that D_p, D_s have a range of [0, 1] and resulting from the converter symmetry and power direction, D_φ is varied within [0, 0.5]. Besides, in order to ensure that the converter works in voltage boosting situation, $D_p > D_s$ is necessary from the point of realizing soft-switching for all switches in the DAB converter, which will be demonstrated in the following paragraph. $D_p + D_s > 1$ is also predefined so that the converter can transmit relatively higher power.

$$\begin{cases} i_L(t_1)=2\left(D_s-kD_p\right)\le 0\\ i_L(t_2)=4kD_\varphi+\left(2-2k\right)D_s\ge 0\\ i_L(t_3)=4kD_\varphi-\left(2-2k\right)D_s\le 0\\ i_L(t_4)=-2\left(D_s-kD_p\right)\ge 0 \end{cases} \tag{6}$$

$$\begin{cases} i_L(t_1)=2\left(D_s-kD_p\right)\ge 0\\ i_L(t_2)=2\left(D_s-kD_p\right)\le 0\\ i_L(t_3)=4kD_\varphi+\left(2-2k\right)D_s\ge 0\\ i_L(t_4)=4D_\varphi-\left(2-2k\right)D_p\ge 0 \end{cases} \tag{7}$$

$$\begin{cases} i_L(t_1)=4-4D_\varphi-\left(2+2k\right)D_p\le 0\\ i_L(t_2)=\left(2+2k\right)D_s+4k\left(D_\varphi-1\right)\ge 0\\ i_L(t_3)=4kD_\varphi+\left(2-2k\right)D_s\ge 0\\ i_L(t_4)=4D_\varphi-\left(2-2k\right)D_p\ge 0 \end{cases} \tag{8}$$

TABLE I. Output Power, Backflow Power and Inductor Peak Current for Each Opearation Mode

	P_o	P_{back}	$I_{L,peak}$
Mode I	$4kD_sD_\varphi$	$\begin{bmatrix}0.5(1-k)\left(kD_p-D_s\right)^2+0.5(1-k)^2D_s^2\\-2k(1-k)D_sD_\varphi+2k^2D_\varphi^2\end{bmatrix}\Big/(1-k)$	$2(1-k)D_s+4kD_\varphi$
Mode II	$2k\begin{bmatrix}\left(D_p+D_s-D_\varphi\right)\cdot D_\varphi\\-0.25\left(D_p-D_s\right)^2\end{bmatrix}$	$\frac{\left(D_s-kD_p\right)^2}{2}$	$2(1-k)D_s+4kD_\varphi$
Mode III	$k\begin{bmatrix}4D_\varphi\left(1-D_\varphi\right)\\-\left(1-D_s\right)^2-\left(1-D_p\right)^2\end{bmatrix}$	$\frac{k\left[\left(1+k\right)D_p-2\left(1-D_\varphi\right)\right]^2}{2k+2}$	$2(1-k)D_s+4kD_\varphi$

TABLE II. SOFT-SWITCHING CONSTRAINTS AND POWER TRANSFER RANGE FOR EACH OPERATION MODE

	Mode boundaries	Soft-switching constraints	Power transfer range
Mode I	$0 < D_\varphi \le \frac{D_p - D_s}{2}$	$\frac{2k}{1-k} D_\varphi \le D_s \le kD_p$	$0 < P_o \le 2k^2(1-k)\cdot D_p^2$
Mode II	$\frac{D_p - D_s}{2} < D_\varphi \le 1 - \frac{D_p + D_s}{2}$	$D_s = kD_p, \quad D_\varphi \ge \frac{1-k}{2} D_p$	$2k^2(1-k)\cdot D_p^2 < P_o$ $\le (-2k)\cdot\left[\left(k^2+k+1\right)D_p^2 - (2k+2)D_p + 1\right]$
Mode III	$1 - \frac{D_p + D_s}{2} < D_\varphi \le \frac{1}{2}$	$\begin{cases} 0 < D_s \le kD_p, & D_\varphi \ge 1 - \frac{1+k}{2k} D_s \\ kD_p < D_s < 1, & D_\varphi \ge 1 - \frac{1+k}{2} D_p \end{cases}$	$(-2k)\cdot\left[\left(k^2+k+1\right)D_p^2 - (2k+2)D_p + 1\right]$ $< P_o \le k\left(2D_p - D_p^2\right)$

On the other hand, in order to achieve soft-switching for all switches in the converter, the leakage inductance current at the switching instant should follow the rules as expressed in (6), (7) and (8). By solving them, the soft-switching constraints can be obtained for Mode I, Mode II and Mode III, respectively. The results are summarized in the third column of Table II.

Depending on the common limits, the mode boundaries and the soft-switching constraints on the three control variables D_p, D_s and D_φ, the power transfer range of the DAB converter can be developed in different operating modes. Along with the respective transmission power expression in Table I, the minimum and maximum power transfer can be calculated for Mode I, Mode II and Mode III and the results are listed in the last column of Table II.

It can be seen that the power transfer range for each mode is dependent on the voltage ratio k and the duty cycle of the primary voltage D_p. Furthermore, based on the calculated results, Fig. 3 illustrates the power transfer range for each operation mode as a function of [k, D_p]. In the three figures, the lower blue surface is the minimum transmission power while the upper red surface represents the maximum power surface. From Fig. 3(a) to Fig. 3(c), it can be concluded that the converter can operate under different output power ranges from light loading up to heavy load conditions.

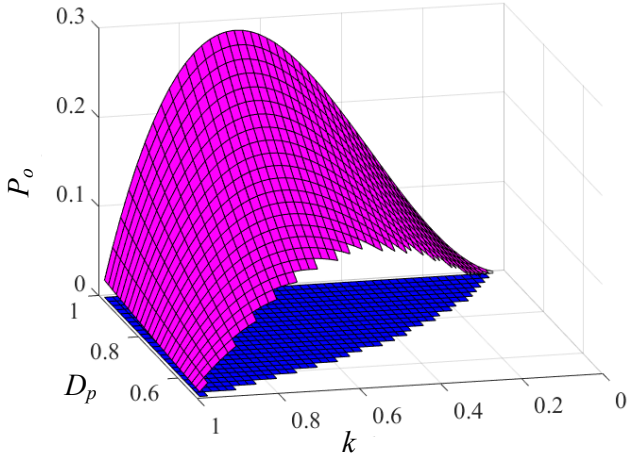

(a)

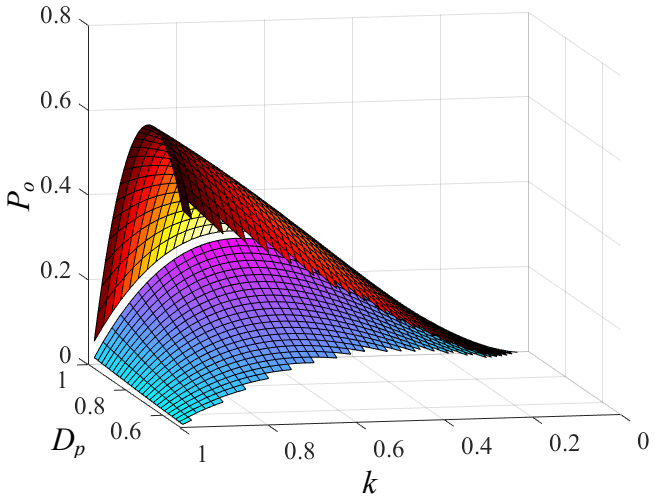

(b)

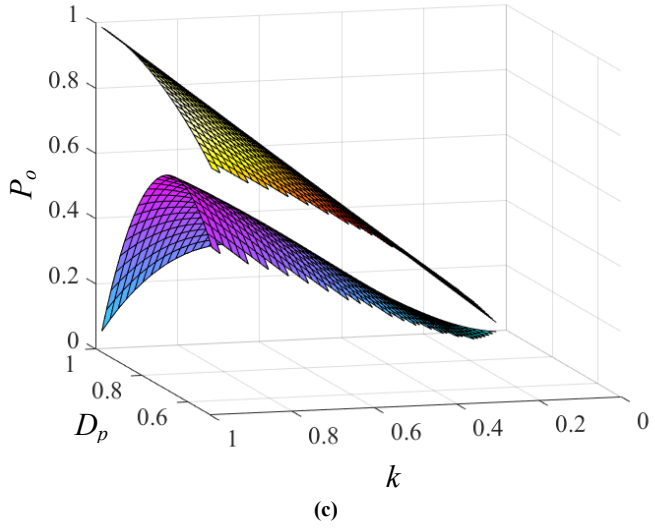

(c)

Fig. 3 Power transfer range for each operation mode with respect to the voltage ratio k and the duty cycle of the primary voltage D_p: (a) Mode I (b) Mode II (c) Mode III. For all the three operation modes, the cool and hot color map denote the minimum and maximum power transfer surfaces, respectively.

IV. Backflow Power and Peak Current Optimization

Seen from the transmission power expressions in Table I, there are infinite combinations of [D_p, D_s, D_φ] for each operation mode to achieve the same power level. Because of this, it is possible to simultaneously reduce the backflow power and the peak inductance current by means of selecting the optimal combination of these three control variables.

Firstly, for the purpose of reducing the average backflow power, taking Mode III as an example, the optimal analytical solution of D_p can be achieved through the partial differential of P_{back}, as expressed by (9).

$$D_p = \frac{2\left(1-D_\varphi\right)}{1+k} \tag{9}$$

It should be noted that the optimization is conducted for a reference output power. See the expression of the average output power in Table I and replace D_p with (9), the expression can be rewritten as

$$P_o = k\left[4D_\varphi\left(1-D_\varphi\right)-\left(1-D_s\right)^2-\left(\frac{1-k-2D_\varphi}{1+k}\right)^2\right] \tag{10}$$

Comparing (10) and the expression of the peak inductance current in Table I, both of them are the function of D_s and D_φ, which means that for a certain output power, there is an optimal combination of [D_s, D_φ] to accomplish the goals of minimizing the peak current and simultaneously satisfying the output power level. In order to find the analytical solution of D_s, the phase-shift angle D_φ is expressed in the explicit function of [D_s, P_o] according to (10), which is

$$D_\varphi = \Big[k^3+k^2+2k- \left(1+k\right)\sqrt{k\left(2k^2+2k-\left(k^2+2k+2\right)\left[k\left(1-D_s\right)^2+P_o\right]\right)}\Big] \Big/ \left[2k\left(k^2+2k+2\right)\right] \tag{11}$$

Then substituting (11) into the expression of $I_{L,peak}$ in Table I, the following (12) can be obtained as the function of D_s.

$$I_{L,peak} = \Big[4+4k+\left(2k^3+2k^2-4\right)\left(1-D_s\right)- 2\left(1+k\right)\sqrt{k\left(2k^2+2k-\left(k^2+2k+2\right)\left[k\left(1-D_s\right)^2+P_o\right]\right)}\Big] \Big/ \left(k^2+2k+2\right) \tag{12}$$

Combining (12) and (10), it can be derived that when D_s is equal to

$$D_s = \frac{\left(2k^3+2k^2-4\right)D_\varphi+2+2k^2}{k\left(k+1\right)^2} \tag{13}$$

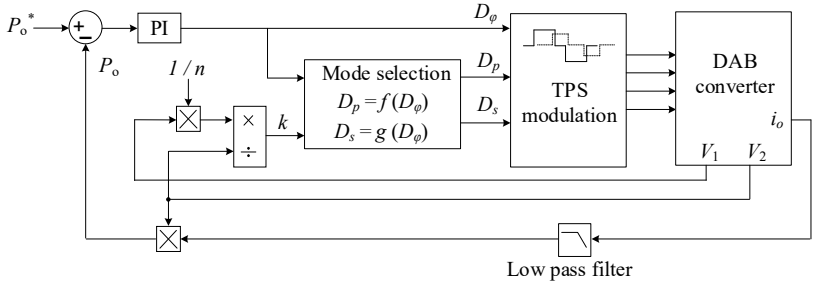

Fig. 4 Block diagram of the proposed optimal control scheme

TABLE III. Relation Expressions of Optimal Control Variables for Each Operation Mode

	Optimal relation expressions	Joint variable limits
Mode I	$D_p = \frac{2D_\varphi}{1-k} \quad D_s = \frac{2kD_\varphi}{1-k}$	$D_\varphi \le \frac{D_p-D_s}{2}, \quad \frac{2k}{1-k}D_\varphi \le D_s \le kD_p$
Mode II	$D_p = \frac{2D_\varphi}{1+3k} \quad D_s = \frac{2kD_\varphi}{1+3k}$	$\frac{1-k}{2}D_p \le D_\varphi \le 1-\frac{1+k}{2}D_p, \quad D_s = kD_p$
Mode III	$D_p = \frac{2\left(1-D_\varphi\right)}{1+k} \quad D_s = \frac{\left(2k^3+2k^2-4\right)D_\varphi+2+2k^2}{k\left(k+1\right)^2}$	$1-\frac{1+k}{2}D_p < D_\varphi \le 0.5, \quad D_s \ge \frac{2k}{1+k}\left(1-D_\varphi\right)$

the minimal peak inductance current is achieved for a reference output power. Therefore, as a function of D_φ and k, (9) and (13) are the optimal D_p and D_s to reduce the backflow power and peak inductance current. In terms of Mode I and II, similar derivation process also can be adopted, and the obtained results are listed in the second column of Table III. Furthermore, the final limits of D_p, D_s and D_φ for each operation mode are also presented in the last column of Table III by joining the mode boundaries and soft-switching constraints in Table II.

The procedure of the proposed control scheme applying to a DAB converter is illustrated in Fig. 4. The actual transmission power P_o is calculated by multiplying V_2 with the average value of the output current i_o, which can be obtained through a low pass filter. Then the error between the reference value P_o^* and actual P_o is used to produce the phase-shift angle D_φ between the two full bridges. At the same time, the operation mode is also selected by comparing the reference power with the three power transfer ranges in Table II.

After the calculation of the voltage ratio k, the values of the other two control variables D_p and D_s can be calculated using the expressions listed in Table III. Together with D_φ, these three control variables are then imported to the TPS modulation module and the switching signals can be generated for the DAB converter accordingly.

V. Experimental Verification

A laboratory prototype shown in Fig. 5 was implemented to verify the effectiveness of the proposed optimized control scheme. The system parameters are listed in Table IV. Taking Mode III as an example, the steady-state operating waveforms of the DAB converter are presented in Fig. 6. v_p and v_s are the voltages generated by the high-voltage side and low-voltage side H-bridge. Since the low-voltage side of the transformer has a larger current than the high-voltage side due to power balance, it will be easier to observe the effect of proposed control scheme on the backflow power reduction. So the waveforms of the secondary current i_s are also shown in Fig. 6.

Fig. 6(a) shows the measured results of the converter under conventional TPS modulation, where the values of the three control variables D_p, D_s and D_φ are selected only based on the reference output power and the soft-switching constraints.

TABLE IV. Parameters for the Experiments

Parameters	Values
High voltage side V_1	100 V
Low voltage side V_2	40 V
Turns ratio of the HF transformer n:1	3.5:1
Switching frequency f_{sw}	60 kHz
Dead time T_{dead}	200 ns
Series inductor L_s	35.9 μH
Leakage inductance of the transformer L_{tr}	17.83 μH

On the other hand, taking the backflow power and peak current reduction into account, Fig. 6(b) shows the measured waveforms of the converter as a result of applying the proposed control scheme into the prototype. The transmission power in these two operating states are both at 400 W. The measured peak value of the inductance current in Fig. 6(a) and Fig. 6(b) is respective 42.35 A and 39.18 A, which validates the effect of the optimized control scheme on reducing the peak current.

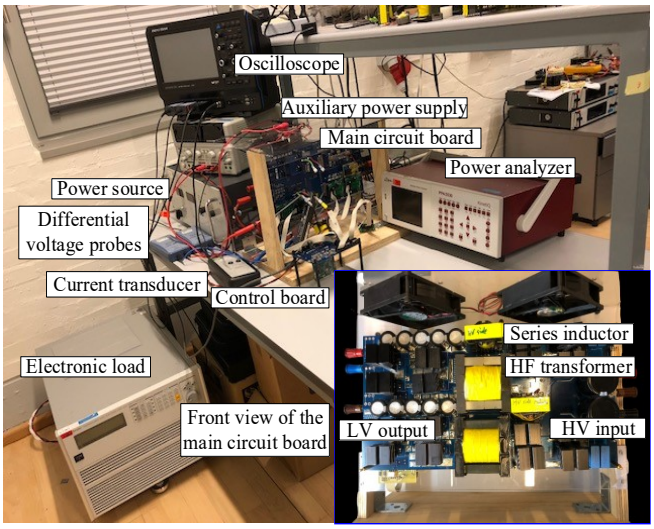

Fig. 5. Test platform for the DAB converter

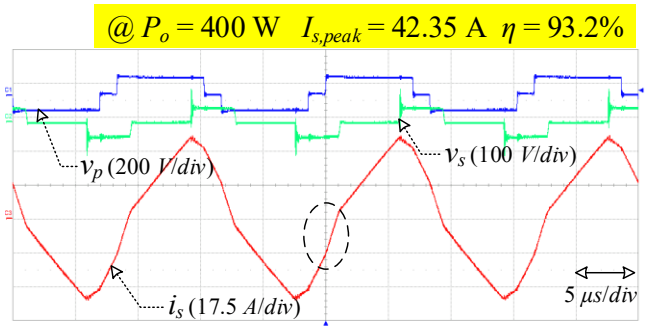

(a)

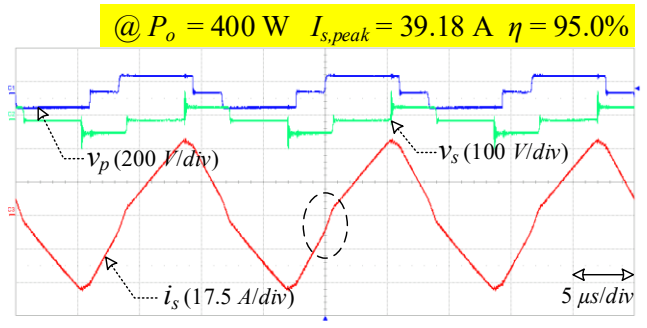

(b)

Fig. 6. Obtained experimental waveforms of DAB converter in Mode III with: (a) conventional control (b) optimized control scheme

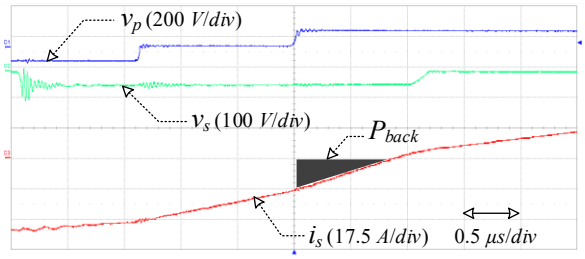

(a)

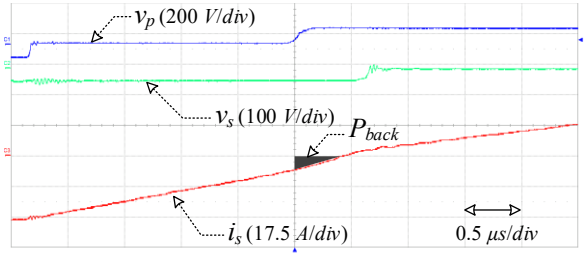

(b)

Fig. 7. Amplified waveforms wrapped by dashed line in Fig. 6(a) and Fig. 6(b), respectively

In order to observe the backflow power, the waveforms wrapped by dashed line in Fig. 6 are amplified by decreasing the time scale, as shown in Fig. 7. It can be seen that the shaded area in Fig. 7(b) is clearly smaller than that in Fig. 7(a), indicating a reduced backflow power in the proposed control scheme. Besides, the system efficiency is also improved from 93.2% to 95.0%, as marked in Fig. 6, which further validates that the proposed optimization scheme can effectively enhance the converter efficiency performance by reducing the backflow power and peak leakage inductance current for the TPS based DAB converter.

VI. Conclusions

This paper proposes an optimized control scheme for DAB converters to reduce the backflow power and peak current based on the TPS modulation. Compared to the conventional method, the proposed control scheme can select the optimal modulation parameters to effectively reduce the backflow power and peak inductance current, thus the system efficiency can be improved and the current stress of the switching devices is decreased. A comprehensive analysis of the soft-switching constraint, power transfer range and optimization process is also explained in detail, which can be further extended to other modulation methods such as DPS and EPS.

References

[1] G. G. Oggier, G. O. García and A. R. Oliva, "Switching Control Strategy to Minimize Dual Active Bridge Converter Losses," in *IEEE Trans. on Power Electronics,* vol. 24, no. 7, pp. 1826 - 1838, 2009.

[2] B. Li, Q. Li, F. C. Lee, Z. Liu and Y. Yang, "A High-Efficiency High-Density Wide-Bandgap Device-Based Bidirectional On-Board Charger," in *IEEE Journal of Emerging and Selected Topics in Power Electronics,* vol. 6, no. 3, pp. 1627 - 1636, 2018.

[3] T. M. Parreiras, A. P. Machado, F. V. Amaral, G. C. Lobato, J. A. S. Brito and B. C. Filho, "Forward Dual-Active-Bridge Solid-State Transformer for a SiC-Based Cascaded Multilevel Converter Cell in Solar Applications," *IEEE Tran. on Industry Applications*, vol. 54, no. 6, pp. 6353 - 6363, 2018.

[4] Z. Wang, B. Liu, L. Guan, Y. Zhang, M. Cheng, B. Zhang and L. Xu, "A Dual-Channel Magnetically Integrated EV Chargers Based on Double-Stator-Winding Permanent-Magnet Synchronous Machines," *IEEE Tran. on Industry Applications*, early access, 2018.

[5] B. Zhao, Q. Yu, and W. Sun, "Extended-phase-shift Control of Isolated Bidirectional DC-DC Converter for Cower Distribution in Microgrid," *IEEE Trans. on Power Electronics*, vol. 27, no. 11, pp. 4667 - 4680, 2012.

[6] H. Bai and C. Mi, "Eliminate Reactive Power and Increase System Efficiency of Isolated Bidirectional Dual-active-bridge DC-DC Converters Using Novel Dual-phase-shift Control," *IEEE Trans. on Power Electronics*, vol. 23, no. 6, pp. 2905 - 2914, 2009.

[7] B. Liu, P. Davari and F. Blaabjerg, "An Optimized Control Scheme for Reducing Conduction and Switching Losses in Dual Active Bridge Converters," in *Proc. IEEE Energy Conversion Congress and* Exposition *(ECCE),* 2018, in press.

[8] B. Liu, P. Davari and F. Blaabjerg, "A Flexible Control Scheme for Single-Stage DAB AC/DC Converters," in *Proc. IEEE International Power Electronics and Application Conference and Exposition (PEAC),* 2018, in press.

[9] K. Wu, C. W. De Silva, and W. G. Dunford, "Stability Analysis of Isolated Bidirectional Dual Active Full-bridge DC-DC Converter with Triple Phase Shift Control," *IEEE Trans. on Power Electronics*, vol. 27, no. 4, pp. 2007 - 2017, 2012.

[10] A. K. Jain and R. Ayyanar, "PWM Control of Dual Active Bridge: Comprehensive Analysis and Experimental Verification," *IEEE Trans. on Power Electronics*, vol. 26, no. 4, pp. 1215 - 1227, 2011.

[11] G. G. Oggier and M. Ordonez, "High Efficiency DAB Converter Using Switching Sequences and Burst-mode," *IEEE Trans. on Power Electronics*, vol. 31, no. 3, pp. 2069 - 2082, 2016.

[12] H. Shi, H. Wen, J. Chen, Y. Hu, L. Jiang, G. Chen and J. Ma, "Minimum-Backflow-Power Scheme of DAB-Based Solid-State Transformer With Extended-Phase-Shift Control," *IEEE Trans. on Industry Applications*, vol. 54, no. 4, pp. 3483 - 3496, 2018.

[13] J. Huang, Y. Wang, Z. Li and W. Lei, "Unified Triple-Phase-Shift Control to Minimize Current Stress and Achieve Full Soft-Switching of Isolated Bidirectional DC–DC Converter," *IEEE Trans. on Industrial Electronics*, vol. 63, no. 7, pp. 4169 - 4179, 2016.

[14] F. Xiong, J. Wu, L. Hao and Z. Liu, "Backflow Power Optimization Control for Dual Active Bridge DC-DC Converters," *Energies*, vol. 10, no. 9, 2017.

[15] F. Krismer and J. W. Kolar, "Closed Form Solution for Minimum Conduction Loss Modulation of DAB Converters," *IEEE Trans. on Power Electronics*, vol. 27, no. 1, pp.174 - 188, 2012.